NEW APPROACH TO ACCURATE FAULT LOCATION AND PHASE SHIFT MEASUREMENTS

M. Kezunović
Texas A&M University

B. Peruničić
Lamar University

U.S.A.

Abstract – Accurate determination of fault location and phase shift are crucial steps in protective relaying and fault analysis on transmission lines as well as in system restoration and economic dispatch control. Major advancements in these areas can be achieved using synchronized sampling and new digital algorithms for fault location and phase shift measurements. This paper introduces new approaches for those measurements using synchronized samples obtained from recording instrumentation interfaced to the Global Positioning System (GPS) of satellites.

Keywords: Fault Location, Phase Shift Calculation, Synchronized Sampling, GPS Satellites

INTRODUCTION

Application of synchronized sampling to various power system monitoring and control functions has been proposed in the early '80s [1]. However, only recent advancements in the methods and uses of the precise time in power systems have enabled more practical studies to be carried out [2]. As a result, several new applications of synchronized sampling have been identified in the control and protection area [3]. Introduction of the recording instrumentation capable of interfacing with the Global Positioning System (GPS) of satellites provided environment for implementation of several new systems for control and protection [4]. This paper summarizes development activities in the areas of fault location and phase shift measurements undertaken at Texas A&M University in the last two years [5–7].

The fault location implementation using synchronized sampling provided a number of advantages over the schemes already proposed. The main improvements are an increased accuracy and an enhanced algorithm robustness. The phase shift measurement using synchronized sampling demonstrates similar properties. Both measurement approaches enable fast calculations making these techniques suitable for both real-time and off-line applications.

The fault location application is discussed first, followed by a discussion of the phase shift measurement. Theoretical algorithm derivations and a brief summary of tests results are given for both applications.

FAULT LOCATION

Theoretical Background

Consider an arbitrary unfaulted three-phase system depicted in Fig. 1. The two ends of the transmission line of interest are labeled S (sending) and R (receiving). The vectors of the phase voltages and currents at the two ends of the transmission line are v_S, i_S, and v_R, i_R, respectively. The length of the line is d. At any location X along the given line, the instantaneous values of the phase voltages and currents are defined as:

$$v_X = v(x,t) = [v_a(x,t), v_b(x,t), v_c(x,t)] \quad (1)$$

$$i_X = i(x,t) = [i_a(x,t), i_b(x,t), i_c(x,t)] \quad (2)$$

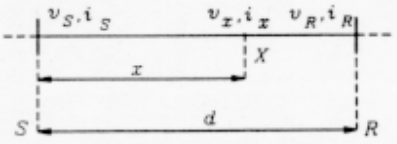

Fig. 1. Unfaulted Three–Phase System

In the case of a homogeneous line (constant line parameters per unit length), the voltages and currents at the end S can be expressed in terms of the voltages and currents at the end R (and vice versa) as:

$$v_R = L^v\{v_S, i_S, d\} \quad (3)$$

$$i_R = L^i\{v_S, i_S, d\} \quad (4)$$

v_S, i_S, and v_R, i_R are vectors defined in the same manner as v_X, i_X (eqs. (1) and (2)). L^v and L^i are linear operators with respect to the vectors of voltages v and currents i.

The relations between voltages and currents at any two points of the transmission line (eqs. (3) and (4)) are not influenced neither by the configuration nor the parameters of the rest of the system of which the line is a part. The particular form of the operators L^v and L^i depends on

the transmission line parameters and its electrical length.

Now, consider the faulted three phase transmission line depicted in Fig. 2. The fault point is denoted as F, and is at a distance x from the line end R.

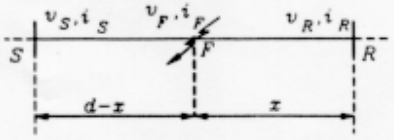

Fig. 2. Faulted Three–Phase Transmission Line

The phase voltages at the fault point F are related to both line ends' phase voltages and currents (eq. (4)):

$$v_F = L^v\{v_S, i_S, d-x\} \quad (5)$$
$$v_F = L^v\{v_R, i_R, x\} \quad (6)$$

where v_F is the vector of instantaneous phase voltages defined in the same way as v_X (eq (1)), and $d-x$ is the distance between the end S and the fault point F.

Because of the continuity of the voltage along the transmission line, eqs. (5) and (6) can be combined, leading to:

$$L^v\{v_S, i_S, d-x\} = L^v\{v_R, i_R, x\} \quad (7)$$

Finally, consider a hypothetical unfaulted three–phase transmission line having the same characteristics as the faulted one. This line is depicted in Fig. 3. The point F on this hypothetical unfaulted line is at the same location as the fault point F on the faulted line (Fig. 2). The vectors of phase voltages and currents of the hypothetical line are defined as for the case of the faulted line.

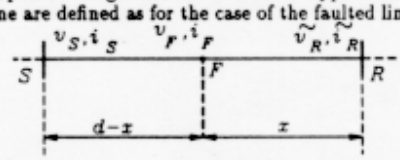

Fig. 3. Hypothetical Three–Phase Transmission Line

Let us assume that the vectors of voltages and currents at the end S of the hypothetical line are exactly the same as the corresponding ones v_S and i_S on the actual faulted line. Therefore, at the point F on the hypothetical line, the voltages are the same as the corresponding ones on the faulted line. Since the hypothetical line is unfaulted, it is homogeneous over its whole length. Therefore, the end R voltages and currents on the hypothetical line can be expressed, using eqs. (5) and (6) as:

$$\tilde{v}_R = L^v\{v_S, i_S, d\} \quad (8)$$
$$\tilde{i}_R = L^i\{v_S, i_S, d\} \quad (9)$$

The parts of the hypothetical line between the end S and F, and the end R and F, are also homogeneous. Thus, for the point F, expression (7) becomes:

$$L^v\{v_S, i_S, d-x\} = L^v\{\tilde{v}_R, \tilde{i}_R, x\} \quad (10)$$

Due to the assumption that the end S voltages and currents are the same on both the faulted and the hypothetical lines, eqs. (7) and (10) can be combined, leading to:

$$L^v\{v_R, i_R, x\} - L^v\{\tilde{v}_R, \tilde{i}_R, x\} = 0 \quad (11)$$

The linearity of operators L^v and L^i, with respect to the vectors of voltages and currents, enables expression (11) to be rewritten as:

$$L^v\{\Delta v_R, \Delta i_R, x\} = 0 \quad (12)$$

where Δv_R and Δi_R are defined as:

$$\Delta v_R = v_R - \tilde{v}_R$$
$$\Delta i_R = i_R - \tilde{i}_R$$

Equation (12) is a *generic fault location equation*. It relates the unknown distance x to the fault point F and the mismatch of the phase voltages and currents, Δv_R and Δi_R. The mismatches Δv_R and Δi_R contain both line ends' voltage and current values. While v_R and i_R are the measured vectors at one end, $\tilde{v}_R$ and $\tilde{i}_R$ are the calculated ones. The vectors $\tilde{v}_R$ and $\tilde{i}_R$ are calculated using the measured values of the other line end, v_S and i_S (eqs. (8) and (9)). Therefore, the generic equation (12) implicitly relates the unknown distance x to the fault point F, and both the line ends' instantaneous phase voltages and currents, v_S, i_S, and v_R, i_R.

For a particular transmission line, the generic equation (12) has a unique form that determines the way it can be solved for an unknown fault location. In the case of a short line, the equation can be solved in an explicit form. For a long line, the equation is solved in an indirect way.

Performance Evaluation

The performances of both the short and long–line algorithms were evaluated using EMTP gen-

erated data. Two test systems were modeled using the EMTP, one for testing the short-line algorithm, the other for testing the long-line algorithm. Both test systems are models of actual power systems. Test system 1 is a 161 kV power system with a short transmission line used for testing. The one-line diagram of system 1 is shown in Fig. 4. The transmission line of interest is the one between buses 2 and 3.

The other test system (system 2) is 345 kV with a long transmission line considered for testing the fault location algorithm for the long lines. The transmission line of interest is untransposed and 195 miles long. The one-line diagram of system 2 is shown in Fig. 5. The transmission line of interest is between buses 1 and 2.

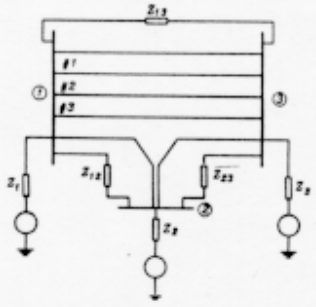

Fig. 4. One-Line Diagram of System 1

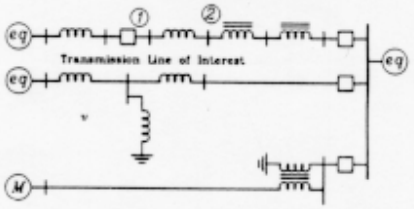

Fig. 5. One-Line Diagram of System 2

The test cases were generated by varying the following four parameters of the fault event: fault location, type of fault, fault resistance, and incidence angle of the fault occurrence.

The error of the fault location algorithms was observed for a variety of fault cases. The error (%) of the fault location algorithm is defined as:

$$\text{Error}\,(\%) = \frac{|\text{act. fault loc.} - \text{calc. fault loc.}|}{\text{total line length}} \times 100$$

Typical test results for the short and the long line are given in Tables I and II, respectively. More elaborate test results are provided in references [5,6].

The results indicate that the error is rather small for all cases, as it never exceeds 0.75%. Moreover, typical errors are 0.5% for the most common fault type, namely, the line to ground fault. Such a small error is achieved under varying fault characteristics which confirms the robustness of the algorithms.

Table I. Error (%) of the Short-Line Fault Location Algorithm for a Phase A to Ground Fault

Location of Fault	0.1		0.5		0.8	
Incidence Angle (deg)	0	90	0	90	0	90
$R_f = 3\Omega$	0.4344	0.4346	0.2901	0.2093	0.0388	0.0390
$R_f = 50\Omega$	0.4576	0.4549	0.2237	0.2229	0.0464	0.0472

Table II. Error (%) of the Lhort-Line Fault Location Algorithm for a Phase A to Ground Fault

Location of Fault	0.1		0.5		0.8	
Incidence Angle (deg)	0	90	0	90	0	90
$R_f = 3\Omega$	0.4283	0.4212	0.3912	0.3966	0.4783	0.4152
$R_f = 50\Omega$	0.4301	0.4832	0.3991	0.4003	0.4853	0.4765

MEASUREMENT OF PHASE SHIFT

Theoretical Background

The building blocks of the algorithm are bilinear and quadratic forms of signal samples introduced by the authors in [8]. The bilinear form of two discrete signals x_n and y_n is defined as:

$$BFHXY(n) = \sum_{k=0}^{N-1} \sum_{m=0}^{N-1} h_{km} x_{n-k} y_{n-m} \qquad (13)$$

The quadratic form of a discrete signal x_n is defined as:

$$QFHX(n) = \sum_{k=0}^{N-1} \sum_{m=0}^{N-1} h_{km} x_{n-k} x_{n-m} \qquad (14)$$

In these expressions, x_n and y_n are sample sequences of two signals $x(t)$ and $y(t)$ taken in times n/f_s, where f_s is the sampling frequency.

For two signals that are pure sinusoids of the same frequency, f, x_n and y_n have the following values:

$$x_n = X\cos(\delta n + \psi)$$
$$y_n = Y\cos(\delta n + \phi)\ ;\ \delta = 2\pi\frac{f_s}{f} \qquad (15)$$

The value of any bilinear or quadratic form obtained using samples of sinusoidal waveforms consist of two terms, one is constant and the other is oscillating with the frequency of $2f$. The oscillating term is equal to zero when the weight matrix $\{h_{km}\}$ satisfies the condition:

$$\sum_{k=0}^{N-1}\sum_{m=0}^{N-1} h_{km}e^{-jk\delta}e^{-jm\delta} = 0 \qquad (16)$$

In the general case, the above condition is satisfied only for a particular value of δ. However, if the sums of anti-diagonals in the weight matrix are all equal to zero, the condition (16) is satisfied for any value of δ [8]. This is a very convenient property if the frequency of the signal varies. For this reason, only such weight matrices are used for the algorithm presented in this paper.

The constant terms of bilinear and quadratic forms have the following values [9]:

$$BFHXY = \propto(\delta)\frac{X}{2}\cos(\psi-\phi) + \beta(\delta)\frac{XY}{2}\sin(\psi-\phi) \qquad (17)$$

$$QFHX = \propto(\delta)\cdot\frac{X^2}{2} \qquad (18)$$

Coefficients $\propto(\delta)$ and $\beta(\delta)$ are dependent on angle δ and weight matrix elements h_{km}:

$$\propto(\delta) = \sum_{x=0}^{N-1}\sum_{m=0}^{N-1} h_{km}\cos(m-k)\delta \qquad (19)$$

$$\beta(\delta) = \sum_{k=0}^{N-1}\sum_{m=0}^{N-1} h_{km}\sin(m-k)\delta \qquad (20)$$

The phase shift is calculated combining bilinear and quadratic forms in the following expression:

$$\psi-\phi = \sin^{-1}\left\{\frac{BFH_1XY(n)}{\sqrt{QFH_2X(n)\cdot QFH_3Y(n)}}\right\} \qquad (21)$$

Weight matrices H_1, H_2 and H_3 have sums of their anti-diagonals equal to zero, and they also satisfy two additional conditions:

$$\propto_1(\delta) = 0 \qquad (22)$$

$$\beta_1^2(\delta) = \propto_2(\delta)\cdot\propto_3(\delta) \qquad (23)$$

Any three matrices satisfying the above conditions may be used for the calculation of the phase shift.

The expression (21) holds only if amplitudes, frequency and phases of the same signals are constant. If these signal parameters vary in time, then expression (17) holds only if their variations are sufficiently slow so that they may be neglected in the data window.

Performance Evaluation

Two types of computer simulation tests were performed to verify the algorithm. The aim of the first type of tests was to prove that algorithm properties hold if signals are sinusoids with constant or slow varying parameters. For this type of test, samples were defined as follows:

$$x_n = A(n)\cos[\delta(n)n + \psi(n)] \qquad (24)$$
$$y_n = B(n)\cos[\delta(n)n] \qquad (25)$$

The particular functions used for $A(n)$, $B(n)$, $\delta(n)$ and $\psi(n)$ in (24) and (25), as well as test outcomes for the first type of tests, are presented in Table III.

Table III. Test Results

Test	$A(n)$ p.u.	$B(n)$ p.u.
1	1	1
2	1	1
3	1	1
4	$1+0.1\cos(0.01\pi n)$	1
5	1	1
6	1	1

Test	$f(n)$ Hz	f_s kHz	$\psi(n)^o$
1	60	12	45
2	60	60	45
3	60	0.240	45
4	$30+\frac{n}{40}$	12	45
5	60	12	$45-\frac{n}{500}$
6	60	12	$30+\frac{\sqrt{n}}{10}$

Tests #1, #2, and #3 were designed to demonstrate that the algorithm may be used for an arbitrary sampling frequency. Therefore, in these tests, only the sampling frequency was changed. The results were absolutely unaffected by the sampling frequency choice.

The algorithm is also transparent to changes in the value of amplitude and system frequency, as long as these parameters are constant in the data window. If these changes are sufficiently slow, the error is not significant.

In the test #4, the amplitude of the first signal was modulated with a subharmonic having 10% amplitude of the main signal and a frequency of 6 Hz. The frequency of both signals had a linear change of 1 Hz per cycle. Although the changes were significant from the point of view of the system, the algorithm showed quite an accurate value of the phase shift.

The goal of test #5 was to show the dynamic properties of the algorithm. In this test, only the phase shift was varied. Other parameters were kept constant. The algorithm results gives a small error.

In test #6, the phase shift was changed linearly for 60° in 10 cycles. The measurement is expressed as sine of the shift. The results followed the true phase shift with a delay equal to a fraction of a cycle.

The second type of test demonstrated the robustness of the algorithm using EMTP simulation of voltages taken at two transmission line ends during a BC fault. The EMTP model used for this test is the one shown in Figure 4.

The EMTP generated voltage signals were filtered using a four state low pass Butterworth filter to reduce the higher frequency components induced by the fault. The simulated fault changed the phase shift between voltages for 8 degrees. The algorithm output was smooth and a new stationary value was established in the course of one cycle.

Detailed results of all the tests are further discussed in reference [8].

CONCLUSIONS

The results of the study reported in this paper lead to the following conclusions:

- Synchronized sampling enables new approaches to measurements of a fault location and a phase shift.
- The fault location algorithm developed using synchronized sampling offers greater accuracy and robustness than any of the previously published techniques.
- The phase shift measurement approach using synchronized sampling offers an accurate and robust result that is transparent to any constant or slow moving fundamental frequency and signal amplitudes.
- Both fault location and phase shift measurements are obtained in a very short time interval and can be used for real-time monitoring, control and protection applications.

ACKNOWLEDGEMENTS

The authors wish to acknowledge financial support for this study that came from the NASA Grant administered by the Center for Space Power at Texas A&M University. Thanks are also due to Dr. A. D. Patton and Dr. F. E. Little from the Center for Space Power for their interest in, and support of the project.

REFERENCES

[1] P. Bonanomi, "Phase Angle Measurements with Synchronized Clocks – Principle and Applications," *IEEE Transactions on Power Apparatus and Systems*, Vol. PAS-100, No. 12, December 1981.

[2] R. E. Wilson, "Methods and Uses of Precise Time in Power Systems," *Transactions on Power Delivery*, Vol. 7, No. 1, January 1992.

[3] IEEE Working Group Report, Power System Relaying Committee, "Synchronized Sampling and Phasor Measurements for Relaying and Control," *IEEE Transactions on Power Delivery*, Vol. 9, No. 1, January 1994.

[4] Macrodyne, Inc. Clifton Park, New Jersey, U.S.A., "Phasor Measurement Unit – Model 1690," *Application Performance Data Sheet*, 1993.

[5] M. Kezunović, et. al., "An Accurate Fault Location Algorithm Using Synchronized Sampling," *Electric Power Research Journal*, 1994 (Accepted for publication).

[6] M. Kezunović, et. al., "Accurate Fault Location Using Synchronized Sampling at Two Ends of a Transmission Line," *11th PSCC*, Avignon, France, 1993.

[7] M. Kezunović, et. al., "Measurements of Phase Shift Using Synchronized Sampling," *Conference on Precise Measurements in Power Systems*, Washington, D. C., October 1993.

[8] B. Peruničić, et. al., "Bilinear Form Approach to Synthesis of a Class of Electric Circuit Digital Signal Processing Algorithms," *IEEE Transactions on Circuits and Systems*, Vol. 35, No. 9, October 1988.

[9] M. Kezunović, et. al., "Digital Signal Processing Algorithms for Power Quality Assessment," *IECON '92*, San Diego, California, November 1992.